Modelization of combined radiative and conductive heat transfer in three-dimensional complex enclosures

Kamel Guedri
Ecole Nationale d'Ingénieurs de Monastir, Monastir, Tunisie
Mohamed Naceur Borjini
Faculté des Sciences de Monastir, Monastir, Tunisie
Habib Farhat
Institut Préparatoire aux Etudes d'Ingénieurs de Monastir, Monastir, Tunisie

Received March 2003
Revised January 2004
Accepted March 2004

Abstract

Purpose – To provide a finite volume code, based on Cartesian coordinates, for studying combined conductive and radiative heat transfer in three-dimensional irregular geometries.

Design/methodology/approach – In the present study, a three-dimensional blocked-off-region procedure was presented and implemented in a numerical code based on the finite volume method to model combined conductive and radiative heat transfer in complex geometries. This formulation was developed and tested in three-dimensional complex enclosures with diffuse reflective surfaces and containing gray absorbing-emitting and isotropically scattering medium. This approach was applied to analyze the effect of the main of thermoradiative parameters on the temperature and flux values for three-dimensional L-shaped enclosure.

Findings – The proposed isotropic model leads to satisfactory solutions with comparison to reference data, which entitles us to extend it to anisotropic diffusion cases or to non-gray media. The blocked-off-region procedure traits both straight and curvilinear boundaries. For curved or inclined boundaries, a fine or a non-uniform grid is needed.

Originality/value – This paper offers a simple Cartesian practical technique to study the combined conductive and radiative heat transfer in three-dimensional complex enclosures with both straight and curvilinear boundaries.

Keywords Heat transfer, Radiation, Finite volume methods

Paper type Research paper

Nomenclature

a, b	= defined quantities, equations (7a)-(7f) and (16a)-(16i)	L_+	= total number of discrete solid angles oriented to a given boundary
G	= incident intensity $(= \int I \, d\Omega)$	M	= a large number $(M = 10^{20})$
I	= radiant intensity	N	= dimensionless quantity defined in equation (15)
I^0	= black body radiant intensity	N_{cr}	= conduction-radiation parameter defined in equation (4)
L	= total number of discrete solid angles		

International Journal for Numerical Methods in Heat & Fluid Flow
Vol. 15 No. 3, 2005
pp. 257-276

0961-5539
DOI 10.1108/09615530510583874

N_θ, N_φ = number of discrete angles in polar θ, and azimuthal φ directions
$\boldsymbol{n}$ = unit vector normal to the control volume surface
$\dot{q}$ = internal heat source
$\boldsymbol{q}_c$ = dimensionless conductive heat flux
$\boldsymbol{q}_r$ = dimensionless radiative heat flux
$\boldsymbol{q}_t$ = dimensionless total heat flux
r = aspect ratio
R = source term defined in equation (14)
s = distance in the direction Ω of the intensity
S_c, S_{cC}, S_{cP} = additional source terms defined in equation (22)
S_r, S_{rC}, S_{rP} = additional source terms defined in equation (18)
T = temperature
x, y, z = Cartesian coordinates

Greek symbols

β = extinction coefficient ($\beta = \sigma_s + \kappa$)
ΔA = area of a control volume face
Δv = control volume
$\Delta\Omega$ = control solid angle
ε = emissivity
κ = absorption coefficient
σ = Stefan-Boltzmann constant
σ_s = scattering coefficient
θ, ϕ = polar and azimuthal angles, respectively
ω = scattering albedo ($\omega = \sigma_s/\beta$)
Ω = unit vector in direction of intensity

Subscripts

e, w, n, s, f, b = faces of control volume centered in P
E, W, N, S, F, B = nodes around the nodal point P
P = nodal point
W = boundary of the computational domain

Superscripts

l, l' = discrete angular directions

1. Introduction

The calculation of radiative heat transfer, in a multidimensional and complex enclosure, demands a numerical technique flexible enough to deal with the irregular geometries. Three of the most adopted methods to treat complex geometries are the discrete ordinates, the discrete transfer and the finite volume methods. The discrete ordinates method (DOM) was adapted to the finite element method by Fiveland (1984) and Fiveland and Jesse (1995) and then formulated with the blocked-off-region procedure by Chai *et al.* (1993). The discrete transfer method (DTM) was used with the cell-blocking procedure based on Cartesian coordinates (Malalasekera and Lockwood, 1991), the finite element method formulation (Meng *et al.*, 1993), and later with non-orthogonal grid systems (Malalasekera and James, 1996). The finite volume method (FVM) was developed with the spatial-multi-block procedure (Chai and Moder, 1997), the blocked-off-region procedure (Chai *et al.*, 1994) and curvilinear elliptic-cylinder and bicylindrical coordinates (Borjini *et al.*, 1999a, b). Chai *et al.* (1995), Lee *et al.* (1996) and Baek *et al.* (1998) applied this method to non-orthogonal coordinate system. Liu *et al.* (1997) formulated both FVM and DOM in general body-fitted coordinates. These three methods were employed by Coelho *et al.* (1998) to predict radiative heat transfer in enclosures containing obstacles of very small thickness (baffles). In this reference, the FVM and the DOM was developed using the blocked-off-region procedure, and more studies concerning radiative heat transfer in

enclosures with obstacles, such as protrusions and obstructions are cited. Detailed bibliography on modeling radiative heat transfer in complex geometries can be found in the work of Henson and Malalasekera (1997).

In the present study, the blocked-off-region procedure is implemented in an existing numerical code based on the FVM (Borjini *et al.*, 1999a) to model combined conductive and radiative heat transfer in irregular geometries. The new code is tested in three-dimensional illustrative examples. Results for purely radiating medium are given for three-dimensional rectangular and L-shaped enclosures. Then the combined conduction and radiation heat transfer in three-dimensional L-shaped enclosure is studied. The enclosure has gray or black diffuse walls and contains a gray, absorbing-emitting and eventually isotropically scattering medium. The effect of the main of thermoradiative parameters on the temperature and flux values is put in evidence.

2. Formulation

The energy equation can be expressed as follows

$$\nabla \cdot \boldsymbol{q}_{\mathrm{r}} = \lambda \nabla^2 T \tag{1}$$

where λ is the thermal conductivity and the divergence of the radiative heat flux $\boldsymbol{q}_{\mathrm{r}}$ is given by

$$\nabla \cdot \boldsymbol{q}_{\mathrm{r}} = 4\pi\kappa \left[I^0(T) - \frac{1}{4\pi} \int_{\Omega=4\pi} I(s,\Omega)\, \mathrm{d}\Omega \right] \tag{2}$$

By introducing the following dimensionless variables and parameters:

$$\begin{gathered} T^* = \frac{T}{T_{\mathrm{ref}}}, \quad x^* = \frac{\beta x}{\tau_W}, \quad y^* = \frac{\beta y}{\tau_L}, \quad z^* = \frac{\beta z}{\tau_H}, \quad \tau_W = \beta W, \quad \tau_L = \beta L, \\ \tau_H = \beta H, \quad r_{xy} = W/L, \quad r_{xz} = W/H, \quad I^* = \frac{I}{\sigma T_{\mathrm{ref}}^4} \end{gathered} \tag{3}$$

The energy equation (1) can then be rewritten as

$$\frac{1}{\tau_W} \left(\frac{\partial^2 T^*}{\partial x^2} + r_{xy}^2 \frac{\partial^2 T^*}{\partial y^2} + r_{xz}^2 \frac{\partial^2 T^*}{\partial z^2} \right) = \frac{4\kappa}{N_{\mathrm{cr}}} \left[T^{*4} - \frac{1}{4} \int_{\Omega=4\pi} I^*(s,\Omega)\, \mathrm{d}\Omega \right] \tag{4}$$

where

$$N_{\mathrm{cr}} = \frac{\lambda\beta}{\sigma T_{\mathrm{ref}}^3 W}$$

is the conduction-radiation parameter with κ and β are the absorption and the extinction coefficients of the medium.

For simplicity, the superscript * denoting the normalized quantity is omitted.

The dimensionless directional heat flux is defined as following:

$$\boldsymbol{q}_{\mathrm{t}} = \boldsymbol{q}_{\mathrm{c}} + \boldsymbol{q}_{\mathrm{t}} = -\frac{4N_{\mathrm{cr}}}{\tau_{x_i}}\frac{\partial T}{\partial x_i}n_i + \int_{\Omega=4\pi} I(s,\Omega)\Omega\,\mathrm{d}\Omega \tag{5}$$

where the first and the second terms on the right-hand side are dimensionless conductive and radiative heat fluxes, respectively.

By integrating equation (4) over control volume, the following equation can be written

$$a_P T_P = a_W T_W + a_E T_E + a_S T_S + a_N T_N + a_B T_B + a_F T_F + b_P \tag{6}$$

The equation (6) can be rewritten as

$$T_P = \frac{a_W T_W + a_E T_E + a_S T_S + a_N T_N + a_B T_B + a_F T_F + b_P}{a_W + a_E + a_S + a_N + a_B + a_F + (S_m)_P} \tag{7a}$$

where

$$a_W = a_E = \frac{1}{\tau_W}\frac{\Delta y \Delta z}{\Delta x} \tag{7b}$$

$$a_S = a_N = \frac{r_{xy}^2}{\tau_W}\frac{\Delta x \Delta z}{\Delta y} \tag{7c}$$

$$a_B = a_F = \frac{r_{xz}^2}{\tau_W}\frac{\Delta x \Delta y}{\Delta z} \tag{7d}$$

$$a_P = a_W + a_E + a_S + a_N + a_B + a_F + 4\Delta v\frac{\kappa}{N_{\mathrm{cr}}}T_P^3 \tag{7e}$$

$$b_P = \Delta v_P\frac{\kappa}{N_{\mathrm{cr}}}\left[\int_{\Omega=4\pi} I(s,\Omega)\,\mathrm{d}\Omega + 3T_P^3\right] \tag{7f}$$

$$(S_m)_p = 4\Delta v_P\frac{\kappa}{N_{\mathrm{cr}}}T_P^3 \tag{7g}$$

The radiative transfer equation for absorbing-emitting and isotropically scattering medium, is written as

$$\frac{\partial I(s,\Omega)}{\partial s} + \beta I(s,\Omega) = \beta R \tag{8}$$

where

$$R = (1-\omega)I^0(s) + \frac{\omega}{4\pi}\int_{4\pi} I(s,\Omega')\,\mathrm{d}\Omega' \tag{9}$$

$I(s,\Omega)$ is the radiation intensity in the direction Ω at the position s. I^0 is the blackbody radiation intensity.

The boundary condition on the gray diffuse wall with the prescribed temperature T_b can be denoted by

$$I(s,\Omega) = \varepsilon I^0(s) + \frac{(1-\varepsilon)}{\pi}\int_{\Omega'\cdot\boldsymbol{n_w}<0} I(s,\Omega')|\Omega'\cdot\boldsymbol{n_w}|\,\mathrm{d}\Omega' \tag{10}$$

2.1 The finite volume method

The finite-volume method for radiative heat transfer divides the computational domain into finite number of control volumes and the total solid angle into arbitrary number of solid angles. The control solid angle $\Delta\Omega^l$ was calculated analytically by

$$\Delta\Omega^l = \int_{\theta^{l-}}^{\theta^{l+}}\int_{\varphi^{l-}}^{\varphi^{l+}} \sin\theta\,\mathrm{d}\theta\,\mathrm{d}\varphi \tag{11}$$

The integration of equation (8) over an arbitrary control volume Δv and a control angle $\Delta\Omega^l$ gives

$$\int_{\Delta\Omega^l}\int_{\Delta A} I\Omega\cdot\boldsymbol{n}\,\mathrm{d}A\,\mathrm{d}\Omega = \int_{\Delta\Omega^l}\int_{\Delta v}\beta(R-I)\,\mathrm{dv}\,\mathrm{d}\Omega \tag{12}$$

By assuming constant the magnitude of the intensity but allowing its direction to vary within the control volume and control angle, the following finite-volume formulation can be obtained

$$\sum_{i=1}^{6} I_i^l \Delta A_i N_i^l = \beta(R - I^l)\Delta v \tag{13}$$

with

$$R = (1-\omega)I^0 + \frac{\omega}{4\pi}\sum_{l'=1}^{L} I^{l'}\Delta\Omega^{l'} \tag{14}$$

The term N_i^l, evaluated analytically, takes into account the variation of the intensity direction within $\Delta\Omega^l$,

$$N_i^l = \frac{1}{\Delta\Omega^l}\int_{\Delta\Omega^l}\Omega\cdot\boldsymbol{n_i}\,\mathrm{d}\Omega \tag{15}$$

Equation (13) indicates that a net outgoing radiant energy across the control-volume faces must be balanced by a net generation of radiant energy within the control volume and control angle.

Using the step scheme (Chai *et al.*, 1995) equation (8) becomes

$$a_P^l I_P^l = a_W^l I_W^l + a_E^l I_E^l + a_S^l I_S^l + a_N^l I_N^l + a_B^l I_B^l + a_F^l I_F^l + b_P \tag{16a}$$

where

$$a_W^l = \Delta A_w \max\left[-N_w^l, 0\right] \tag{16b}$$

$$a_E^l = \Delta A_e \max\left[-N_e^l, 0\right] \tag{16c}$$

$$a_S^l = \Delta A_s \max\left[-N_s^l, 0\right] \tag{16d}$$

$$a_N^l = \Delta A_n \max\left[-N_n^l, 0\right] \tag{16e}$$

$$a_B^l = \Delta A_b \max\left[-N_b^l, 0\right] \tag{16f}$$

$$a_F^l = \Delta A_f \max\left[-N_f^l, 0\right] \tag{16g}$$

$$\begin{aligned} a_P^l = {} & \Delta A_w \max\left[N_w^l, 0\right] + \Delta A_e \max\left[N_e^l, 0\right] + \Delta A_s \max\left[N_s^l, 0\right] \\ & + \Delta A_n \max\left[N_n^l, 0\right] + \Delta A_b \max\left[N_b^l, 0\right] + \Delta A_f \max\left[N_f^l, 0\right] + \beta \Delta v_P \end{aligned} \tag{16h}$$

$$b_P = \beta R_P \Delta v_P \tag{16i}$$

The radiative boundary condition (equation (10)) for a diffusely emitting and reflecting wall can be discretized as

$$I_W^l = \frac{\varepsilon \sigma T_W^4}{\pi} + \frac{(1-\varepsilon)}{\pi} \sum_{L_+} \left| N_w^{l'} \right| I_W^{l'} \Delta \Omega^{l'} \tag{17}$$

2.2 The blocked-off-region procedure

In order to avoid the complexity of treating non-orthogonal grids, it is suitable to formulate a procedure to model irregular geometries using Cartesian coordinates formulation.

The blocked-off-region procedure consists on drawing nominal domains around given physical domains (Figure 1). The new domain contains *active* and *inactive* regions for which the solutions are sought. This procedure has been developed for conductive and convective heat transfer (Patankar, 1980) then extended to two-dimensional radiative transfer problem by Chai *et al.* (1993, 1994). The model that we will present now is a three-dimensional formulation of this approach.

In order to distinguish active cells from inactive ones, an additional source term is suggested

$$S_r = S_{rc} + S_{rP} I_p^l \tag{18}$$

and added to the right member in equation (9). Equations (16h) and (16i) become, respectively,

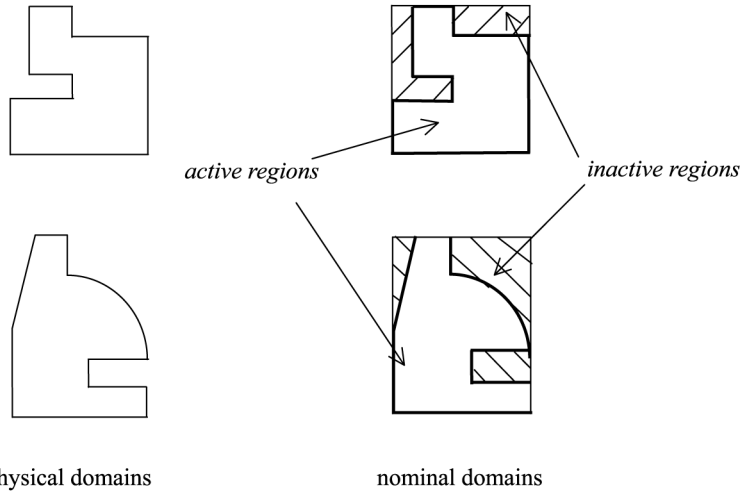

Figure 1.
2D Illustrative example of nominal and physical domains

$$a_p^l = \Delta A_w \max\left[N_w^l, 0\right] + \Delta A_e \max\left[N_e^l, 0\right] + \Delta A_s \max\left[N_s^l, 0\right] + \Delta A_n \max\left[N_n^l, 0\right] + \Delta A_b \max\left[N_b^l, 0\right] + \Delta A_f \max\left[N_f^l, 0\right] + (\beta - S_{rP})\Delta v_{\mathrm{p}} \tag{19}$$

$$b_p = (\beta R_p + S_{rc})\Delta v_p \tag{20}$$

For a given real black boundary, the additional source term is chosen as follows: $(S_{rc}, S_{rp}) = (0, 0)$ for the active region and $(MI^0, -M)$ for the inactive region (M is a large number). For real gray boundaries, we distinguish between emitted and reflected intensities (Chai *et al.*, 1994) and for the inactive cells the additional source terms become $(\varepsilon MI^0, -M)$ for the emitted part. The reflected part is added directly into the active region calculation of the control volumes adjacent to the real boundaries. Using equation (18), the additional source terms can be written, for control volume surfaces orthogonal to the x-axis, as follows

$$S_{rc} = \frac{N_w^l \Delta y}{\Delta v_P} \frac{(1-\varepsilon)}{\pi} \sum_{L_+} \left| N_w^{l'} \right| I_W^{l'} \Delta \Omega^{l'}$$
$$S_{rP} = 0 \tag{21}$$

Similar equations can be written for the control volume surfaces orthogonal to the y- and z-axis. In this work the step scheme is used for all control volumes. Other scheme may be used only in the active region. In inclined or curved geometries the boundaries are approximated with stepped profiles. Therefore, to get a reasonably accurate solution a finer grid or a non-uniform grid is needed.

For the energy equation, the blocked-off-region technique consists on introducing a source term in the discretized energy equation

$$S_c = S_{cC} + S_{cP} T_P \tag{22}$$

where S_{cC} and S_{cP} are constants. The energy discretized equation becomes

$$T_P = \frac{a_W T_W + a_E T_E + a_S T_S + a_N T_N + a_B T_B + a_F T_F + [b_P + S_{cC}]}{a_W + a_E + a_S + a_N + a_B + a_F + [(S_m)_P - S_{cP}]} \tag{23}$$

For all *active* control volume $S_{cC} = S_{cP} = 0$ but in the *inactive* region, those coefficients are given by

$$S_{cC} = MT_{\mathrm{b}}$$

and

$$S_{cP} = -M \tag{24}$$

This condition forces the nodal temperature of the *inactive* control volumes to

$$T_P \approx \frac{MT_{\mathrm{b}}}{M} = T_{\mathrm{b}} \tag{25}$$

Consider the situation shown in Figure 2(a), when the control volume centred on P is adjacent to an isothermal real boundary from the South, the additional source term in equation (23) must be written as

$$S_{cC} = a_S T_{\mathrm{b}}$$

and

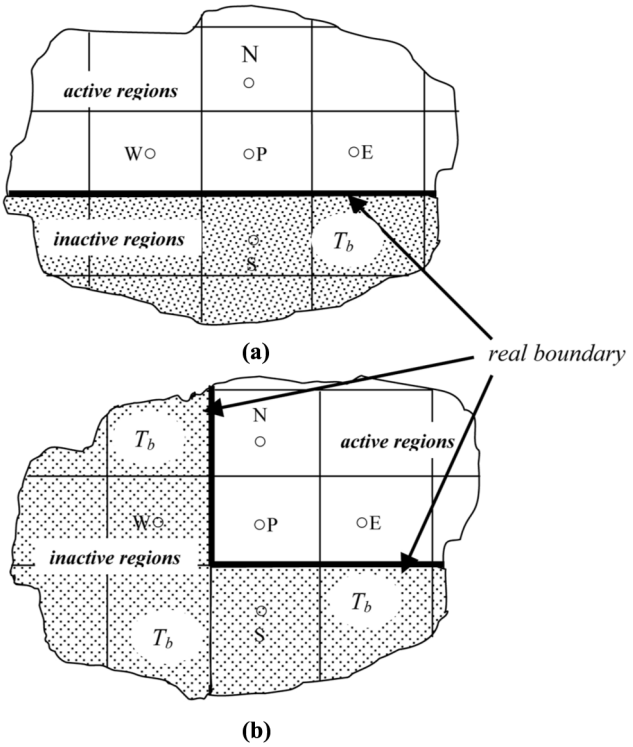

Figure 2.
Particular real boundary conditions

$$S_{cP} = -a_S \tag{26}$$

For the situation shown in Figure 2(b), when the control volume P is limited by two isothermal real boundaries at the South and the West walls, those coefficients are specified as

$$S_{cC} = a_S T_b + a_W T_b$$

and

$$S_{cP} = -a_S - a_W \tag{27}$$

3. Radiative test cases

The following test cases are defined for the three-dimensional rectangular and L-shaped enclosures. The angular and spatial meshes are specified as one goes along. The calculus process is stopped when the radiation intensity field satisfies for each node P and direction l

$$\frac{\left|I_P^{l(n)} - I_P^{l(n-1)}\right|}{I_P^{l(n)}} \leq 10^{-5} \tag{28}$$

where n is the number of iteration.

3.1 Three-dimensional rectangular enclosure

As the first test problem, the FVM is applied to the three-dimensional idealized furnace (Figure 3) proposed by Mengüç and Viskanta (1985). The dimensional size of the computational domain is $W \times H \times L = 2 \times 2 \times 4\,m^3$. The six gray walls are submitted to prescribed thermo-radiative conditions $(T, \varepsilon) = (1,200\,K,\ 0.85)$ for the wall $z = 0$, $(400\,K,\ 0.7)$ for the wall $z = H$ and $(900\,K,\ 0.7)$ otherwise. First the furnace is filled with a gray absorbing-emitting gas with $\kappa = 0.25/m$, $\kappa = 0.5/m$ and $\kappa = 1/m$ then with absorbing-emitting and isotropically scattering gas with $\beta = 0.5/m$ and $\omega = 0.7$. The uniform internal heat sources are $\dot{q} = 5\,kW/m^3$ and the RTE is coupled with the energy equation as follows

$$\dot{q} = k(4\pi I^0 - G) \tag{29}$$

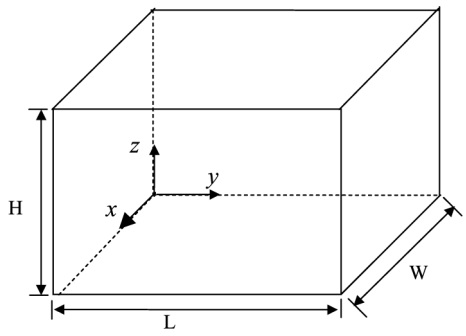

Figure 3.
Three-dimensional idealized furnace

The results obtained with the present finite volume method (FVM) were compared with the zone method predictions (Truelove, 1988). The enclosure is divided into $21 \times 21 \times 21$ spatial mesh, a 4×12 angular mesh for the absorbing-emitting medium and 4×16 angular mesh for the absorbing-emitting and scattering gas.

Figure 4 shows the net radiative flux profiles on the hot and the cold walls of the furnace. Our results are seen to be very close to the zone solution on each wall. The temperature distributions at three axial locations of furnace are shown in Figure 5. The present results show comparable accuracy with those of the zone method. For absorbing-emitting medium a coarser angular and spatial meshes provide sufficient accuracy.

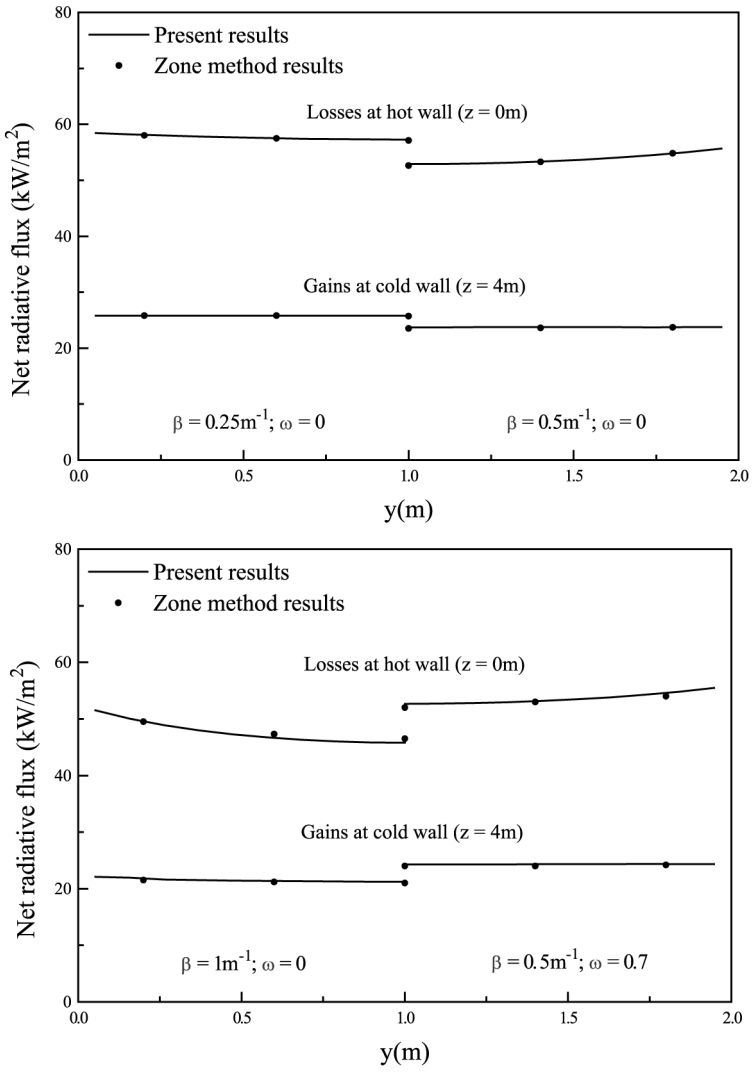

Figure 4.
Net radiative heat fluxes at $z = 0$ and $z = H$ walls

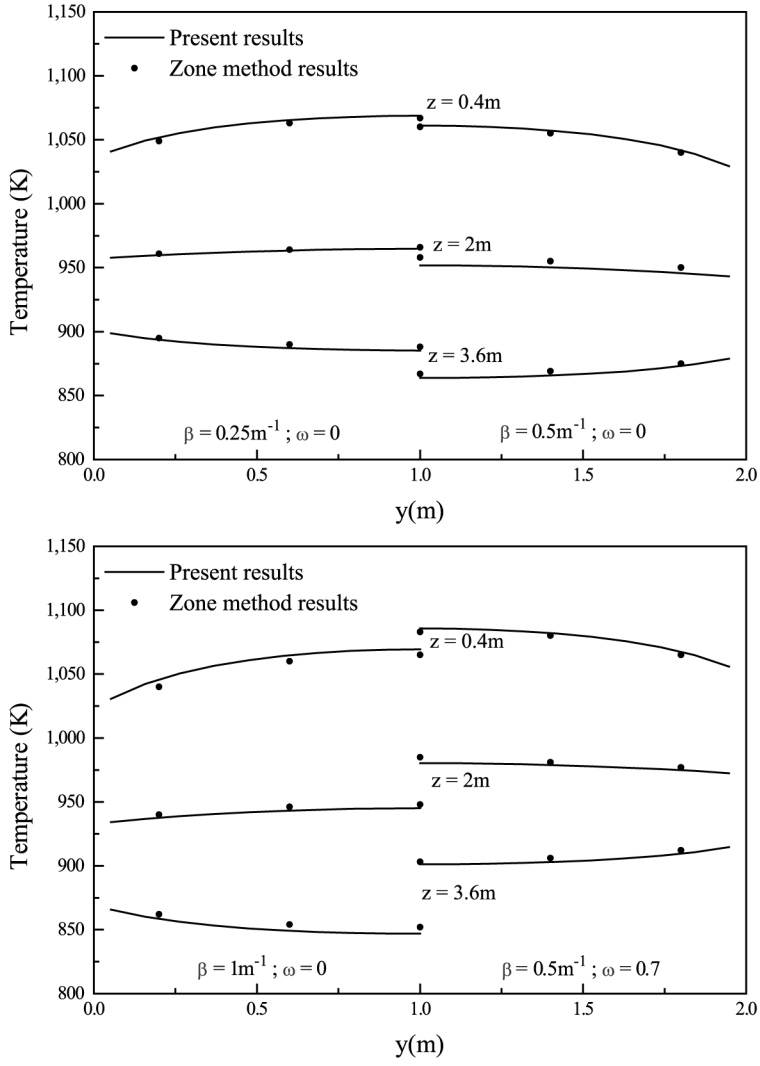

Figure 5.
Gas temperature distributions at three axial locations

3.2 Three-dimensional L-shaped enclosure

The FVM solution of the three-dimensional L-shaped enclosure (Figure 6) is compared with the DTM (Malalasekera and James, 1996) and YIX (Hsu and Tan, 1997) solutions. The dimensions of this tested geometry are $W \times L \times H = 1 \times 3 \times 3\,\mathrm{m}^3$ (where $L_L = 1\,\mathrm{m}$ and $H_L = 2\,\mathrm{m}$). We consider all walls being black at 500 K and an emitting and absorbing media inside at 1,000 K.

For absorption coefficient values of $\kappa = 10, 5, 2, 1$, and 0.5/m, the present model, using a $11 \times 21 \times 21$ spatial mesh and 4×12 angular mesh, gives satisfactory results (Figure 7).

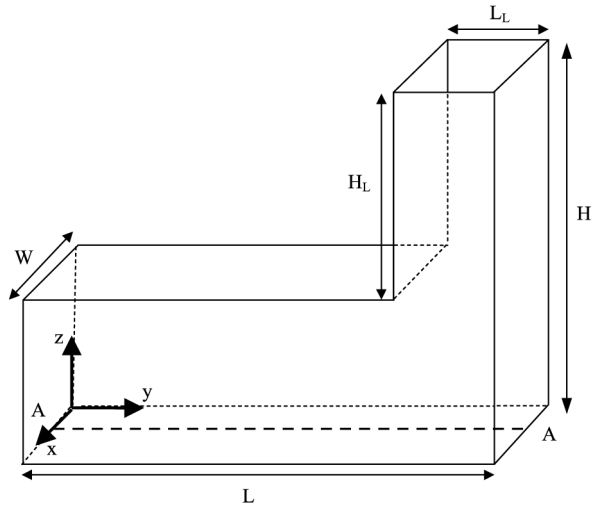

Figure 6.
Three-dimensional L-shaped enclosure

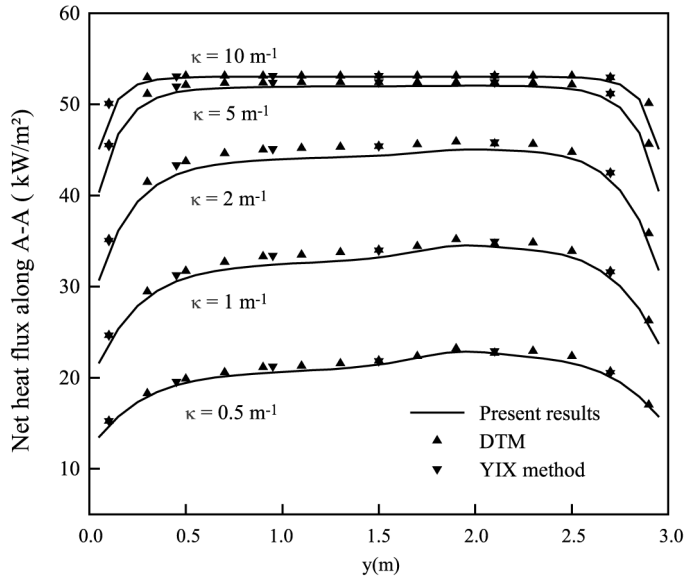

Figure 7.
Radiative heat flux profiles along the line A-A of the L-shaped enclosure

For $\kappa = 10/\mathrm{m}$, the shadowing effect is not likely to propagate down to the bottom surface due to the high optical thickness of the isothermal medium. The curves of low extinction coefficients bring the effect of the protruded volume. Whereas, for strongly absorbing medium, the geometry and shadowing effects on radiative heat transfer are not significant.

The proposed blocked-off-region procedure seems to be an attractive way of dealing with complex enclosures that may be accurately discretized using Cartesian

coordinates, such as the L-shaped enclosure. However, it is a crude approximation in the case of enclosures with curvilinear or skewed boundaries, such as the elliptical and triangular enclosure (results not shown here). In fact, these boundaries need to be treated in a stepwise fashion, and this requires a very fine grid to reduce the numerical errors. In such cases, curvilinear body-fitted coordinates (Liu *et al.*, 1997) will perform better.

4. Combined conduction-radiation heat transfer in 3D L-shaped enclosure

For coupled conduction and radiation heat transfer, the calculus process is stopped when the temperature field satisfies for each node P

$$\frac{\left|T_P^{(n)} - T_P^{(n-1)}\right|}{T_P^{(n)}} \leq 10^{-5} \tag{30}$$

where n is the number of iteration.

The first test deals with a three-dimensional rectangular enclosure as shown in Figure 3. All walls are black where the bottom wall ($z = 0$) being at dimensionless temperature $T = 1$ and the other being at 0.5. This enclosure is filled with an emitting and absorbing medium with $\beta = 1/\text{m}$. In order to get the similar two-dimensional problem reported by Razzaque *et al.* (1984) the dimensions of this tested geometry are $W \times L \times H = 1 \times 1 \times 10/\text{m}^3$.

Figure 8 shows the dimensionless temperature profiles at line $x = W/2$, $y = H/2$ for various conduction-radiation parameters N_{cr}. Using $21 \times 21 \times 11$ control volumes and 4×16 control solid angles, the present results show comparable accuracy with the finite element method solutions (Razzaque *et al.*, 1984).

The dimensions of the three-dimensional L-shaped enclosure (Figure 6) are $W \times L \times H = 1 \times 1 \times 2/\text{m}^3$ (where $L_{\text{L}} = 0.75\,\text{m}$ and $H_{\text{L}} = 1\,\text{m}$). All walls are black where the wall $y = 0$ being at dimensionless temperature $T = 1$ and the other being at 0.5. The calculations have been carried out for several cases to investigate the effects of

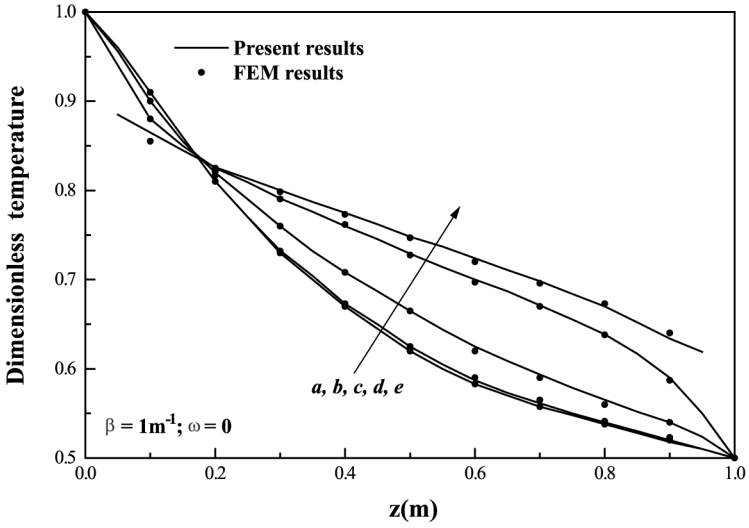

Figure 8.
Dimensionless temperature profiles at line $x = W/2$, $y = L/2$ for various conduction-radiation parameters N_{cr}: (a) conductive heat transfer; (b) $N_{\text{cr}}=1$; (c) $N_{\text{cr}}=0.1$; (d) $N_{\text{cr}}=0.01$; and (e) radiative heat transfer

conduction-radiation parameter N_{cr}, scattering albedo ω and the extinction coefficient β. For all cases, we have considered 4×20 angular mesh, $11 \times 23 \times 23$ spatial mesh and the convergence criterion defined in equation (30).

We consider an absorbing-emitting and non-scattering medium with $\kappa = 1/\text{m}$. Figure 9 shows the dimensionless temperature along the y-direction at the line $x = W/2$ and $z = H/4$ for various values of the conduction-radiation parameters. As N_{cr} decreases, a steeper temperature gradient is formed at both $y = 0$ and $y = L$ walls and the temperature medium far from the hot surface increases. This fact is more clearly reflected in Figure 10 which illustrates the isothermal contours for pure conductive heat transfer, $N_{cr} = 0.01$ and pure radiative heat transfer. In fact, the radiative energy emitted from the hot wall can penetrate more deeply into the medium and is therein transformed into thermal energy (Kim and Baek, 1991). One can note the temperature increasing at the top half of enclosure when N_{cr} rises.

The dimensionless total flux and the wall radiative to total heat flux ratio along the line $x = W/2$, $y = L$ are shown in Figure 11. The total flux becomes evidently much higher as N_{cr} increases and more uniform as N_{cr} decreases. The fractional radiative heat flux is seen to decrease (Figure 11(b)) when N_{cr} increases. The radiative transfer mode is largely predominant in the upper half of the enclosure.

In the following, we fixed the conduction-radiation parameter at $N_{cr} = 0.01$ and we considered an absorbing-emitting and non-scattering medium. Figure 12 illustrates the isothermal contours for various extinction coefficients at plane $x = W/2$. As β increases the temperature at the upper half of the medium increases. The dimensionless total flux and the wall radiative to total heat flux ratio along the line $x = W/2, y = L$ are shown in Figure 13 for various values of the extinction coefficients β. The fractional radiative heat flux is seen to decrease as β increase (Figure 13(b)).

Figure 14 shows the isothermal contours at the plane $x = W/2$ for various scattering albedo values with $N_{cr} = 0.01$ and $\beta = 1/\text{m}$. In the case of purely scattering

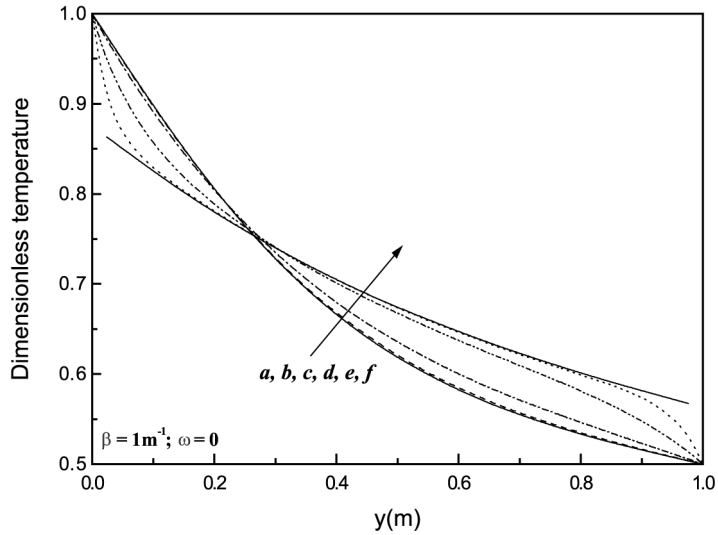

Figure 9.
Dimensionless temperature profiles at line $x = W/2$, $z = H/4$ for various conduction-radiation parameters N_{cr}: (a) conductive heat transfer; (b) $N_{cr}=1$; (c) $N_{cr}=0.1$; (d) $N_{cr}=0.01$; (e) $N_{cr}=0.001$; and (f) radiative heat transfer

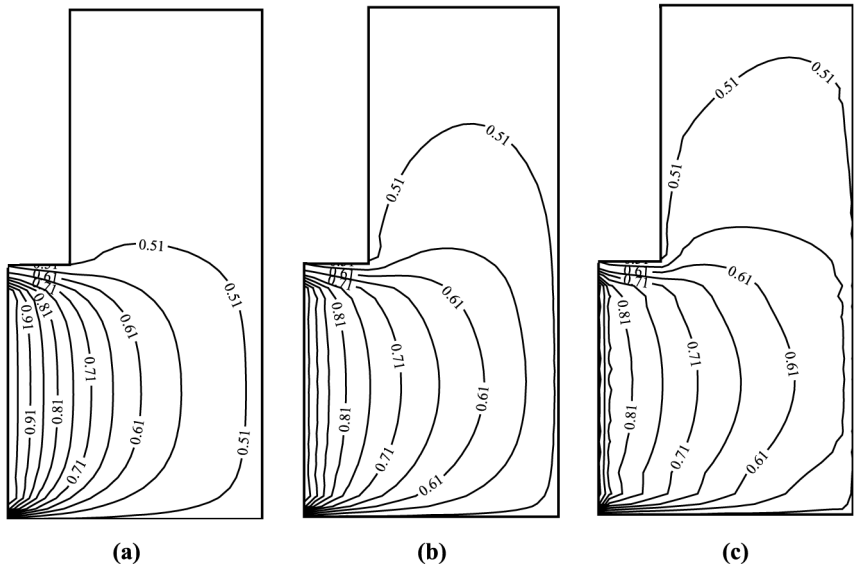

Figure 10.
Isotherms at the plane $x = W/2$ for various conduction-radiation parameters N_{cr}: (a) conductive heat transfer; (b) $N_{cr}=0.01$; and (c) radiative heat transfer

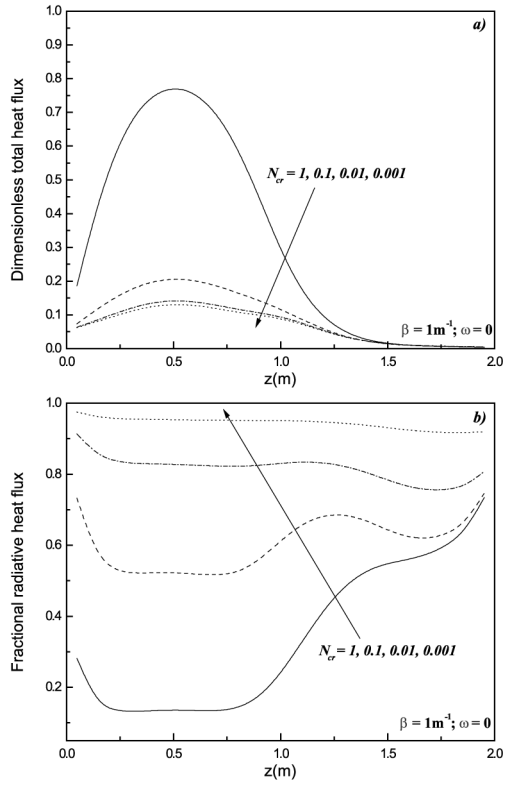

Figure 11.
(a) Dimensionless total heat flux; and (b) fractional radiative heat flux at line $x = W/2$, $y = L$ for various conduction-radiation parameters N_{cr}

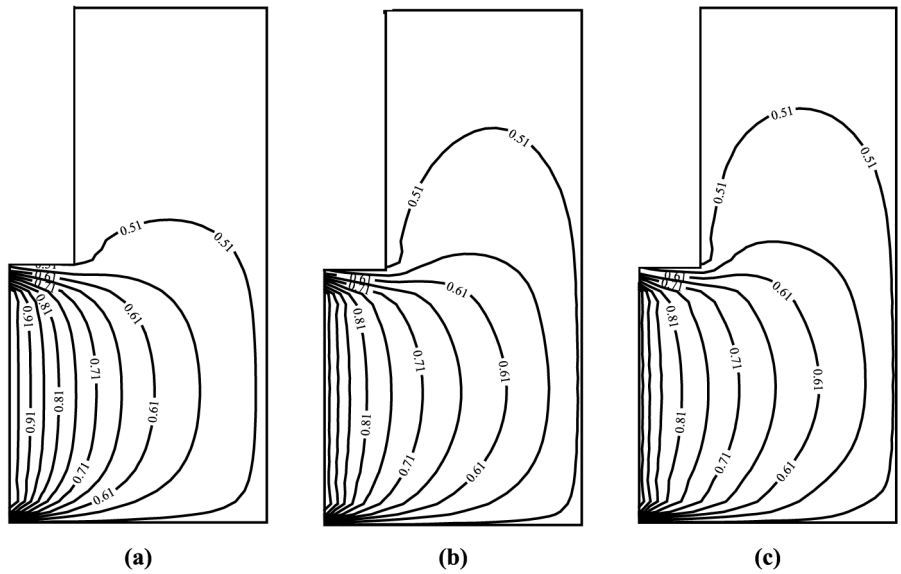

Figure 12.
Isotherms at the plane $x = W/2$ for various extinction coefficients β: (a) $\beta = 0.25$/m; (b) $\beta = 1$/m; and (c) $\beta = 2$/m

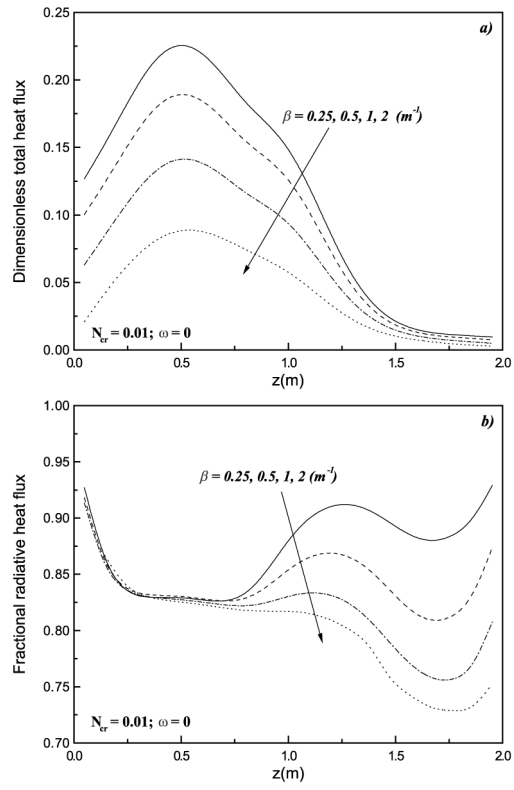

Figure 13.
(a) Dimensionless total heat flux; and (b) fractional radiative heat flux at line $x = W/2$, $y = L$ for various extinction coefficients β

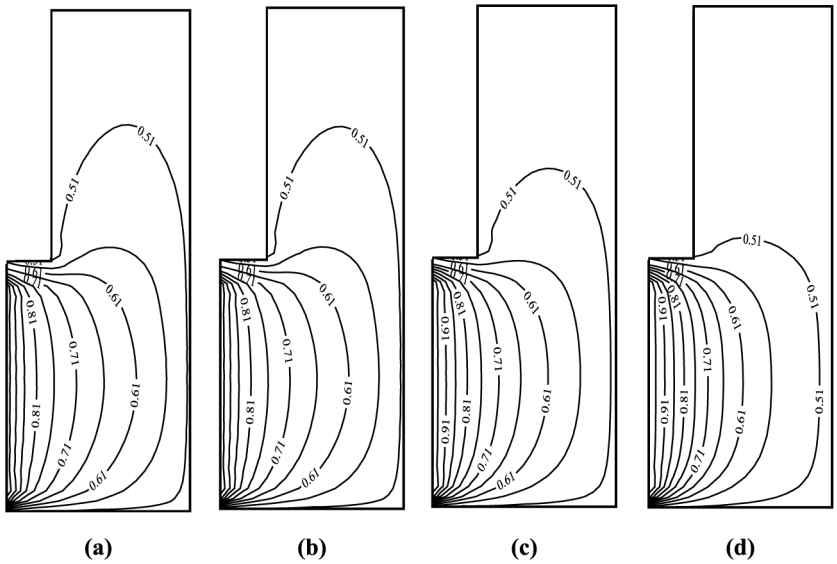

Figure 14.
Isotherms at the plane $x = W/2$ for various scattering albedo coefficients ω: (a) $\omega = 0$; (b) $\omega = 0.2$; (c) $\omega = 0.8$; and (d) $\omega = 1$

medium ($\omega = 1$), the divergence of the radiative heat flux is null, we find the temperature profile for purely conductive heat transfer. The fractional radiative heat flux is seen to increase as ω increases (Figure 15(b)), while the dimensionless total heat flux seems to be insensitive to this parameter (Figure 15(a)).

In the following, the FVM is applied to the L-shaped enclosure plotted in Figure 6 where its dimensions are $W \times L \times H = 1 \times 1 \times 2/\mathrm{m}^3$ and $L_\mathrm{L} = 0.75\,\mathrm{m}$. All walls are assumed to be black where the west wall ($y = 0$) being at dimensionless temperature $T = 1$ and the other being at 0.5. Figures 16 and 17 show the effect of aspect ratio r ($r = H_\mathrm{L}/H$) on the total heat flux and on the isothermal contours for the case of $N_\mathrm{cr} = 0.01$, $\beta = 1/\mathrm{m}$ and $\omega = 0.5$. For all aspect ratio, the maximum of the dimensionless total heat flux is localized at the same height then the centre of the hot surface $z = (H - H_\mathrm{L})/2$ (Figure 16). This is confirmed by the isothermal contours on the mid-plane ($x = W/2$) plotted in Figure 17. Figure 16 also shows clearly the non-linear dependence between the dimensionless total heat flux and the aspect ratio. In fact, this flux decreases enormously when r changes from 1/2 to 3/4.

5. Conclusion

In the first part of this work, the finite volume method formulated with the blocked-off region procedure was developed and tested in three-dimensional complex enclosures with diffuse reflective surfaces and containing gray absorbing-emitting and isotropically scattering medium. Compared with benchmarked results, the finite volume method gives satisfactory predictions of both wall heat flux and temperature distributions. For curved or inclined boundaries, a fine or a non-uniform grid is needed. Chai and Moder (1997) formulated the spatial multi-block procedure, which avoids a fine discretization of the totality of the nominal domain.

In the second part, this approach was applied to analyze the effect of the main of thermoradiative parameters (conduction-radiation parameter, single scattering albedo

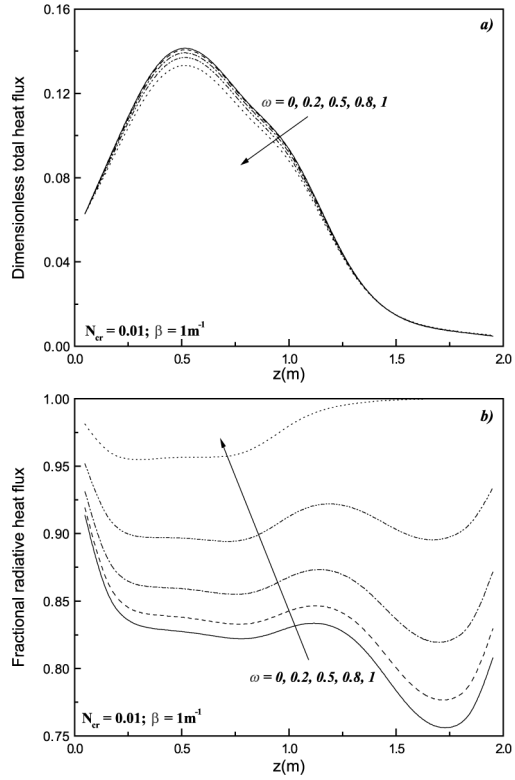

Figure 15.
(a) Dimensionless total heat flux and (b) fractional radiative heat flux at line ($x = W/2, y = L$) for various scattering albedo coefficients ω

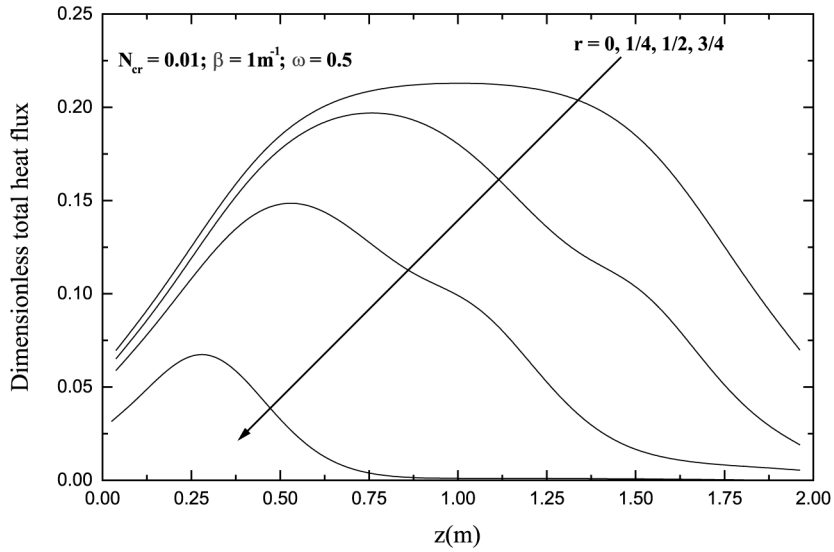

Figure 16.
Dimensionless total heat flux at line $x = W/2, y = L$ for various aspect ratio r ($r = H_L/H$)

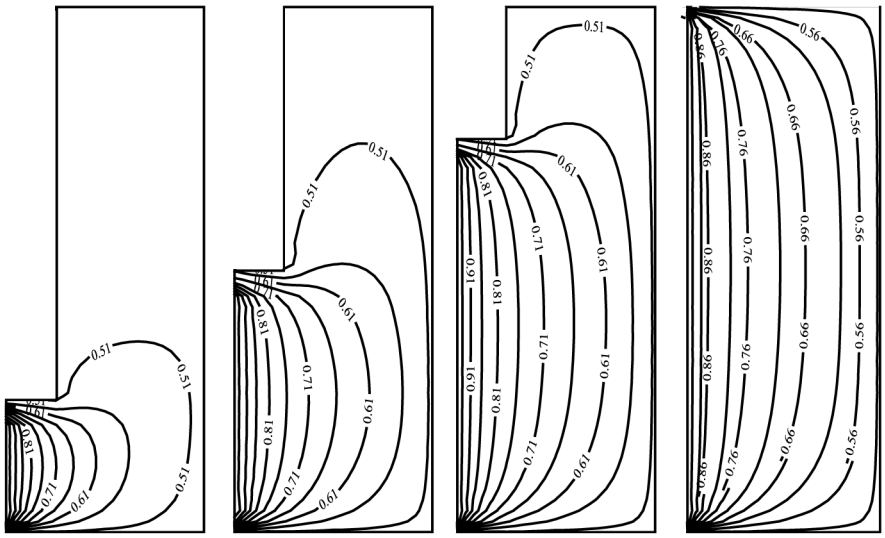

Figure 17.
Isotherms at the plane ($x = W/2$) for various aspect ratio r ($r = H_L/H$): (a) r=3/4; (b) $r = 1/2$; (c) $r = 1/4$; and (d) $r = 0$

and extinction coefficient) on the temperature and flux values for three-dimensional L-shaped enclosure.

The proposed isotropic model leads to satisfactory solutions with comparison to reference data, which entitles us to extend it to anisotropic diffusion cases or to non-gray media.

References

Borjini, M.N., Mbow, C. and Daguenet, M. (1999a), "Numerical analysis of the effect of radiation on laminar steady natural convection in a two-dimensional participating medium between two horizontal cofocal elliptical cylinders", *Numerical Heat Transfer, Part A*, Vol. 35, pp. 467-94.

Borjini, M.N., Mbow, C. and Daguenet, M. (1999b), "Numerical analysis of combined radiation and unsteady natural convection within a horizontal annular space", *International Journal of Numerical Methods for Heat & Fluid Flow*, Vol. 9, pp. 742-64.

Chai, J.C. and Moder, J.P. (1997), "Spatial-multiblock procedure for radiation heat transfer", *Numerical Heat Transfer, Part B*, Vol. 31, pp. 277-93.

Chai, J.C., Lee, H.S. and Patankar, S.V. (1993), "Treatment of irregular geometries using a Cartesian-coordinates-based discrete-ordinates-method", *Radiative Heat Transfer Theory and Application, HTD*, No. 244, pp. 49-54.

Chai, J.C., Lee, H.S. and Patankar, S.V. (1994), "Treatment of irregular geometries using a Cartesian-coordinates finite-volume radiation heat transfer procedure", *Numerical Heat Transfer, Part B*, Vol. 26, pp. 225-35.

Chai, J.C., Parthasarathy, G., Lee, H.S. and Patankar, S.V. (1995), "Finite volume radiative heat transfer procedure for irregular geometries", *Journal of Thermophysics and Heat Transfer*, Vol. 9, pp. 410-5.

Coelho, P.J., Gonçalves, J.M., Carvalhu, M.G. and Trivic, D.N. (1998), "Modelling of radiative heat transfer in enclosures with obstacles", *International Journal of Heat Mass Transfer*, Vol. 41, pp. 745-56.

Fiveland, W.A. (1984), "Discrete ordinates solutions of radiation transport equation of rectangular enclosures", *ASME Journal of Heat Transfer*, No. 106, pp. 699-706.

Fiveland, W.A. and Jesse, J.P. (1995), "Comparison of discrete ordinates formulations for radiative heat transfer in multidimensional geometries", *Journal of Thermophysics and Heat Transfer*, No. 9, pp. 47-54.

Henson, J.C. and Malalasekera, W.M.G. (1997), "Comparison of the discrete transfer and Monte Carlo methods for radiative heat transfer in three-dimensional nonhomogeneous scattering media", *Numerical Heat Transfer, Part A*, Vol. 32, pp. 19-36.

Hsu, P.F. and Tan, Z. (1997), "Radiative and combined-mode heat transfer within L-shaped nonhomogeneous and nongray participating media", *Numerical Heat Transfer, Part A*, Vol. 31, pp. 819-35.

Kim, T.Y. and Baek, S.W. (1991), "Analysis of combined conductive and radiative heat transfer in a two-dimensional rectangular enclosure using the discrete ordinates", *International Journal of Heat and Mass Transfer*, Vol. 34, pp. 2265-73.

Lee, K.H., Lee, J.S. and Choi, M. (1996), "Parametric analysis of radiative-convective heat transfer around a circular cylinder in a cross flow using the finite volume radiation solution method", *Numerical Heat Transfer, Part A*, Vol. 29, pp. 181-96.

Liu, J., Shang, H.M., Chen, Y.S. and Wang, T.S. (1997), "Prediction of radiative transfer in general body-fitted coordinates", *Numerical Heat Transfer, Part B*, Vol. 31, pp. 423-39.

Malalasekera, W.M.G. and James, E.H. (1996), "Radiative heat transfer calculations in three-dimensional complex geometries", *J. Heat Transfer*, Vol. 118, pp. 225-8.

Malalasekera, W.M.G. and Lockwood, F.C. (1991), "Computer simulation of the king's cross fire: effect of radiative heat transfer on fire", *Proc. Inst. Mech. Engineering, Part C*, Vol. 205, pp. 201-8.

Meng, F.L., Mty, F. and Camarero, R. (1993), "Radiative heat transfer by the discrete transfer method using an unstructured mesh", *Radiative Heat Transfer: Theory and Applications, ASME HTD*, Vol. 234, pp. 55-66.

Mengüç, M.P. and Viskanta, R. (1985), "Radiative transfer in three-dimensional enclosures containing inhomogeneous, anisotropically scattering media", *J. Quant. Spectrosc. Radiat. Transfer*, Vol. 33 No. 6, pp. 533-49.

Patankar, S.V. (1980), *Numerical Heat Transfer and Fluid Flow*, McGrawHill, New York, NY.

Razzaque, M.M., Howell, J.R. and Klein, D.E. (1984), "Coupled radiative and conductive heat transfer in a two-dimensional rectangular enclosure with gray participating media using finite element-method", *ASME Journal of Heat Transfer*, Vol. 106, pp. 613-9.

Truelove, J.S. (1988), "Three-dimensional radiation in absorbing-emitting-scattering media using the discrete-ordinates approximation", *J. Quant. Spectrosc. Radiat. Transfer*, No. 39, pp. 27-31.

Further reading

Beak, S.W., Kim, M.Y. and Kim, J.S. (1998), "Nonorthogonal finite-volume solutions of radiative heat transfer in a three-dimensional enclosure", *Numerical Heat Transfer, Part B*, Vol. 34, pp. 419-37.